Article

Discovery Medicine 2024; 36(190): 2191–2201
https://doi.org/10.24976/Discov.Med.202436190.201

Regulation of Ankyrin-G on Nav1.5 Channel in Hypoxic HL-1 Cardiac Muscle Cells

Shanshan Ma[1,†], Shuqin Yang[2,†], Peng Xu[3], Wenshui Li[4], Yang Wang[5], Chenyang Wang[3], Heling Huang[6], Yang Li[7,*], Xuebin Cao[3,*]

[1]Department of Medical Psychology, Hunan Provincial Corps Hospital of the Chinese People's Armed Police Forces, 410006 Changsha, Hunan, China
[2]Department of General Medicine, The 3rd Medical Center of the Chinese PLA General Hospital, 100039 Beijing, China
[3]Department of Cardiology, The 82nd Group Army Hospital of the Chinese PLA, 071000 Baoding, Hebei, China
[4]The National & Local Joint Engineering Laboratory of Animal Peptide Drug Development, College of Life Sciences, Hunan Normal University, 410081 Changsha, Hunan, China
[5]Department of Pharmacy, The Hospital of 96606 Army, 471003 Luoyang, Henan, China
[6]Department of Gynaecology, The 82nd Group Army Hospital of the Chinese PLA, 071000 Baoding, Hebei, China
[7]Department of Cardiology, Chinese PLA General Hospital, 100853 Beijing, China
*Correspondence: liyangbsh@163.com (Yang Li); caoxb252@163.com (Xuebin Cao)
[†]These authors contributed equally.
Published: 20 November 2024

Background: Hypoxia has a major regulatory impact on the electrical activity transmission in the myocardium, and it is involved in the development of tachyarrhythmia disease. Anchor protein G (ankyrin-G, ANK-G) is associated with voltage-gated Na^+ channels (Nav1.5), but its specific role and mechanism have not been fully defined. In this experiment, we investigated the role and mechanism of hypoxia on cardiomyocyte electrophysiology of voltage-gated Na^+ channel, as well as the intervention effect of ankyrin-G by simulating the environment of cardiomyocytes during hypoxia through hypoxia-treated murine atrial myocytes (HL-1).

Methods: The HL-1 cells were divided into 6 groups: normoxia group (NO), hypoxia group (HO), *ANK-G*-overexpressing hypoxia-negative group (ANK-G NC), *ANK-G*-overexpressing hypoxia group (ANK-G), *ANK-G*-silenced hypoxia-negative group (sh*ANK-G* NC), and *ANK-G*-silenced hypoxia group (sh*ANK-G*). *ANK-G* overexpression was induced using lentiviral vectors through the Clustered Regularly Interspaced Short Palindromic Repeats (CRISPR)/Cas9 system. The characteristics of sodium ion channel current (I_{Na}) were observed through the whole-cell patch clamp technique. Western blotting was used to detect the expression of ANK-G and Nav1.5 channel proteins, and the distribution of Nav1.5 channel on HL-1 cells was observed by confocal microscope.

Results: Under hypoxic conditions, the I_{Na} peak current amplitude ($p < 0.01$) and density ($p < 0.01$) of HL-1 cells increased. Compared with the normoxia group, the steady-state inactivation curve of the hypoxia group shifted to the right. The protein levels of ANK-G and Nav1.5 channels were increased under hypoxia ($p < 0.001$). In the ANK-G group, the upregulation of ANK-G protein increased the distribution of Nav1.5 channel in the cell membrane under the hypoxic condition ($p < 0.01$).

Conclusions: Hypoxia increases the I_{Na} amplitude and density of HL-1 cells, and the gating mechanism of I_{Na} is related to steady-state inactivation. Hypoxic condition triggers the upregulation of the ANK-G protein expression, which promotes the redistribution of Nav1.5 channel proteins in the cell membrane, thereby augmenting I_{Na} peak current amplitude and density.

Keywords: HL-1 cells; hypoxia; ankyrin-G; sodium channel current; gating mechanism; atrial fibrillation

Introduction

Atrial fibrillation (AF) is the most common type of cardiac arrhythmia. The main cause of AF is myocardial infarction (MI), and its pathogenic mechanism may be related to hypoxic atrial electrical remodeling, with the main features being the reduction of the effective atrial refractory period and acceleration of atrial conduction [1]. The changes in conduction velocity and refractory period that occur in AF are closely related to the ion channels of the atrial myocytes. A animal study has shown that increased atrial conduction velocity in AF is associated with increased sodium ion channel current (I_{Na}) [2]. Voltage-gated Na^+ channels (Nav1.5) determine the amplitude and slope of the action potential rise, which is particularly important for controlling pulse conduction velocity and maintaining appropriate excitation of the working myocardium [3]. Due to the important role of the cardiac sodium ion channel in cardiac electrical excitability, alterations to its acquired and defective functions lead to the pathogenesis and develop-

ment of a number of cardiac diseases [4,5]. Nav1.5 channel encoded by Sodium Voltage-Gated Channel Alpha Subunit 5 (*SCN5A*) gene is the main voltage-gated Na^+ channel in the heart of vertebrates, and the activity of Nav1.5 channel is the basis for the rapid increase of cardiac action potential, while mutations in human *SCN5A* can lead to functional abnormalities of Nav1.5 channel, which set the stage for sinoatrial node dysfunction, atrial fibrillation, conduction defects, ventricular arrhythmia and other human cardiovascular diseases [6–9]. Myocardial cells are in a hypoxia environment during MI, and hypoxia has been found to cause arrhythmia through the amplification of continuous I_{Na}, which may be related to the mutation of *SCN5A* gene under hypoxia [10]. Therefore, the complexities of hypoxia relating to myocardial infarction underscore the importance to study Nav1.5 channel from multiple angles so as to uncover the mechanism underlying the occurrence and development of AF following myocardial infarction.

Nav1.5 channels are mainly regulated by membrane voltage [11]. Recent studies have found that, like many membrane proteins, Nav1.5 channels are also regulated by a series of protein molecules. These proteins present in the heterocyclic membrane region (such as lateral membrane or intercalated disc region) of cardiomyocytes are involved in the biosynthesis, transportation, localization, activity regulation and degradation of Nav1.5 channel by directly or indirectly acting on different domains of Nav1.5 channel [12]. Among them is anchor protein G (ankyrin-G, ANK-G), which is encoded by ankyrin 3 (*ANK-3*) gene. As a cytoskeleton protein, ANK-G mediates the connection between ion channel complex and blood shadow protein—actin cytoskeleton, and it is an essential myocyte protein for regulating cardiac structure and electrical activity [13]. Expressed in the human heart, ANK-G is located in the myocardial intercalated disc T duct and peripheral sarcolemma membrane, and binds to the conserved region of the intracellular loop in the Nav1.5 II/III homologous domain. Through the recruitment of β-blood shadow protein IV, ANK-G can target the key cardiac signaling molecule—calmodulin-dependent kinase—to the cell intercalated disc, thus playing a key role in the regulation of the number and distribution of Nav1.5 channels in atrial cells [14,15].

We hypothesize that hypoxia experienced by atrial myocytes during myocardial infarction, may result in cardiac sodium channel remodeling, and the effect of ANK-G on Nav1.5 channel target could reverse the occurrence of arrhythmias including AF. Our previous study has found that following exhaustive exercise, the heart would grapple with a state of hypoxia, subjected to increased risk for arrhythmias such as AF. In this study, HL-1 atrial myocyte line was selected and utilized to establish a cellular model of hypoxia, which was then used to study the targeting impact of ANK-G on Nav1.5 channel. Patch clamp technique was used to record the I_{Na} current, and immunofluorescence and Western blotting were used to detect the distribution and expression of Nav1.5 channel protein, which is used to decipher the mechanism of Nav1.5 channel regulation in cardiomyocytes under hypoxia.

Materials and Methods

Cell Line

A murine atrial myocyte line, *i.e.*, HL-1 cells (Huatuo Biotechnology Co., Ltd., Shenzhen, China; article number: HTX2129), was used in this experiment. The cells were tested via Short Tandem Repeat (STR) identification to fulfill the experimental criteria (**Supplementary Material 1**). The HL-1 cells manifest continuous division and spontaneous contraction, while retaining the morphological, biochemical, and electrophysiological characteristics of myocardial cells. Under the conventional adherent cell culture conditions, the cells grew and adopted a morphology resembling fibroblasts (**Supplementary Material 2**).

Materials and Main Instruments

The main reagents used in the present study are listed below. Claycomb Medium (51800C, Sigma, Saint Louis, MO, USA) and fetal bovine serum (TMS-016) were obtained from Sigma (Saint Louis, MO, USA). Trypsin-Ethylenediaminetetraacetic acid (EDTA) digestive fluid (T1320), fibrin (F8180), Dimethyl Sulfoxide (DMSO) (D8371), BCA Protein Concentration Determination Kit (PC002) and sodium dodecyl sulfate polyacrylamide gel electrophoresis (SDS-PAGE) Gel Preparation Kit (P1200) were purchased from Solarbio (Beijing, China). Glutamine (25030081) was purchased from Gibco (Carlsbad, CA, USA). Norepinephrine (HY-13715B) was acquired from MCE company (Rahway, NJ, USA). Nav1.5 antibody (ab300048) was obtained from Abcam (Cambridge, MA, USA). Ankyrin G Monoclonal Antibody (4G3F8) was purchased from Thermo Fisher (Waltham, MA, USA). Beta-actin (bs-0061R) was purchased from Bioss company (Beijing, China). Alexa Fluor 594-Conjugated Goat anti-Rabbit IgG (H+L) (ZF-0516) was obtained from Zhongshan Golden Bridge Company (Beijing, China). Lentivirus (REVG003, LVCON291, LVCON313) was purchased from Gikekian Company (Shanghai, China).

Solutions in the pipette used in this study included: NaCl 5 mmol/L, CsCl 135 mmol/L, EGTA 10 mmol/L, Na2ATP 5 mmol/L, $MgCl_2$ 5 mmol/L, and HEPES 5 mmol/L (pH 7.2). Solutions outside the pipette encompassed: NaCl 30 mmol/L, NMG-Cl 100 mmol/L, $CaCl_2$ 2 mmol/L, $MgCl_2$ 1.2 mmol/L, CsCl 5 mmol/L, HEPES 10 mmol/L, and glucose 5 mmol/L (pH 7.4).

The following main instruments were used in the present study: patch clamp amplifier Ax ONPatch 700B and AID-DIA converter Digidata I322A (Axon, San Jose, CA, USA); borosilicate glass with filament (item#: BF15-86-10, lot number: 158138-4, Sutter, Sacramento, CA, USA); inverted microscope TE300 (Nikon, Tokyo, Japan);

three-dimensional micro manipulator MC1000e (SD, San Francisco, CA, USA); confocal laser microscope SP5 (Leica, Wetzlar, Hessian, Germany); biosafety cabinet and carbon dioxide constant-temperature incubator (Thermo, Waltham, MA, USA); balanced shockproof table (Newport, Irvine, CA, USA); electrophoresis apparatus, electrophoresis tank, and membrane transfer apparatus (BIO-RAD, Hercules, CA, USA); and gel-imaging system (Tanon, Shanghai, China).

Establishment and Grouping of Experiments

This study employed six groups of cells treated differently: normoxia group (NO), hypoxia group (HO), *ANK-G*-overexpressing hypoxia-negative group (ANK-G NC), *ANK-G*-overexpressing hypoxia group (ANK-G), *ANK-G*-silenced hypoxia-negative group (sh*ANK-G* NC), and *ANK-G*-silenced hypoxia group (sh*ANK-G*). NO group was cultured for 2 h in a CO_2 incubator that contained 21% oxygen. Hypoxia group was cultured for 2 h in a three-gas incubator that containing 5% oxygen. The cells were microscopically observed to ensure that they were in good condition. The cells were also tested for mycoplasma contamination.

For the ANK-G group, we generated HL-1 cells overexpressing *ANK-G* using three different guiding sequences of sgRNA: *ANK-3*-sgRNA (seq1, targeting: AAGCATTGGGTATACCCAGG), *ANK-3*-sgRNA (seq2, targeting: TGGGGGTGGTAACGAGAGAT), and *ANK-3*-sgRNA (seq3, targeting: GTAACGAGAGATCGGGTTAC), and inserted GV468 lentivirus constructs separately. The required virus volume was calculated according to the formula:

Virus volume = (multiplicity of infection × number of cells)/virus titer

Taken out of a –80 °C freezer, the raised virus Cas9 was melted on ice. The old culture medium was discarded and replaced with 2.5 mL Claycomb medium (51800C, Sigma, Saint Louis, MO, USA) supplemented with 15% fetal bovine serum (FBS; TMS-016, Sigma, Saint Louis, MO, USA). An infecting enhancer (100 µL) was added to each flask, followed by 10 µL virus, which was gently mixed and incubated at 37 °C for 18 h. The supernatant was discarded, and Claycomb medium containing 15% FBS and 2 µg/mL purinomycin was added for further culture to screen the virus strains. According to the instructions, attaining a transfection rate of 80% is considered successful. The cells were observed under a confocal laser microscope SP5 (Leica, Wetzlar, Hessian, Germany), and then, the cells were continued to be cultured, subcultured and preserved by freezing. The cells that were successfully transfected with Cas9 lentivirus were cultured for 2 h in a hypoxic incubator containing 90% nitrogen prior to subsequent experiments.

For the ANK-G NC group, the HL-1 cells were transfected the same way as those for ANK-G group to induce overexpression of *ANK-G*. The transfected vector was an empty vector without virus.

For the sh*ANK-G* group, we generated *ANK3*-silenced HL-1 cells using a siRNA sequence. *ANK-3*-siRNA sequence (CGCCTGGTAAAGAGACATAAA) was inserted into the GV493 lentivirus construct. The cells were transfected with the lentivirus construct to downregulate the *ANK-G* expression, and cultured for 2 h in an incubator containing 90% nitrogen to simulate hypoxia, prior to subsequent experiments.

For sh*ANK-G* NC group, *ANK-3*-silenced HL-1 cells were generated the same way as those for sh*ANK-G* group. The transfected vector was an empty vector without virus.

Observation and Photography

The cells were inoculated into confocal dishes. Staining was performed when the cells had grown to a confluence of about 60%. Paraformaldehyde (1 mL, 4%) was added to fix the cells after discarding phosphate-buffered saline (PBS), and left to stand at room temperature for 10 min. Then, paraformaldehyde was washed away with PBS, followed by the addition of 1 mL of 0.5% Triton-X100 solution, which permeated through the membrane at room temperature for 10 min. Washing with PBS was performed again, followed by sealing with 1 mL of 3% bovine serum albumin (BSA) and 10% secondary antibody homologous serum for 30 min. Afterward, 5% BSA-diluted primary antibody solution was added and left for overnight incubation at 4 °C. Secondary antibody solution, which was diluted with 5% BSA, was added. Then, the dishes were wrapped with tinfoil and incubated in the dark at room temperature for 30–45 min. The primary antibodies used included those targeting Nav1.5 (1:200; ASC-005, Alomone, Jerusalem, Israel) and ANK-G (1:200; 33-8800, Invitrogen, Carlsbad, CA, USA), and the secondary antibodies Goat Anti-Mouse IgG (1:400 for ab150116, Abcam, Cambridge, MA, USA; and 1:400 for ZF-0516, ZSGB-BIO). The secondary antibody solutions were then discarded and the dishes were washed, prior to observation, coupled with photography, under a confocal microscope SP5 (Leica, Wetzlar, Hessian, Germany). The sealed cell sample could be stored in the refrigerator at 4 °C for more than 2 weeks away from light.

Western Blotting

The cells were lysed by using RIPA lysis buffer (R0020, Solarbio, Beijing, China) for 15–30 min on ice. Each lysate was prepared from lysing 10^6 cells. To extract proteins, 1 mL of the lysate was added with 10 µL of PMSF (100 mM) and 10 µL of cocktail (1:100), shaken well and placed on ice for 15–30 min. The cell fragments and lysate were transferred to the pre-cooled Eppendorf tubes pre-cooled at 4 °C, and then subjected to centrifugation at 12,000 rpm for 20 min. The supernatant was collected for protein concentration determination using BCA kit (PC0020, Solarbio, Beijing, China).

Each protein sample (30 µL) was added with 5× loading buffer (P1040, Solarbio, Beijing, China). After mixing, the sample was boiled for 5 min at 100 °C, and immediately placed in an ice box for rapid cooling. Prior to electrophoresis, 3 µL marker was added to the first well, and 30 µL of denatured protein sample was added into each of the remaining wells in the gel. Electrophoresis was performed at 120 V for 30 min, and then at 150 V for 1 h. Upon completion of electrophoresis, the separated proteins on the gel were transferred to PVDF membranes. The membrane transfer was implemented at a constant current of 200 mA for 2.5 h. Subsequently, the membrane was incubated overnight at 4 °C with primary antibody solutions: beta-actin (1:1000; bs-0061, Bioss, Beijing, China), Nav1.5 (1:1000; ab56240, Abcam, Cambridge, MA, USA), ANK-G (1:1000; 33-8800, Invitrogen, Carlsbad, CA, USA). Afterwards, the membrane was incubated for 1 h with secondary antibody solution (1:5000 for 511103, ZENBIO, Chengdu, Sichuan, China; 1:5000 for ZF-0516, ZSGB-BIO, Chengdu, China). Finally, the membrane was washed and developed. Protein quantitation was performed using ImageJ version 2 (National Institutes of Health, Bethesda, MD, USA).

Examination of Cellular Electrophysiology

While using the microcontroller, the electrode was dipped into the liquid, slowly and vertically. The fluctuation on the display was observed at the same time during electrode dipping. When the signal that the electrode had touched the cells was registered, the resistance was raised 0.1–0.3 MΩ, and the negative pressure was applied until the resistance reached 1 GΩ. Fast capacitance compensation was executed when the signal had stabilized. After sealing, baseline fluctuations were observed on the cell interface to confirm successful membrane rupture induced by rapid or slow suction. The current amplifier of the patch clamp was connected to the computer, and the stimulation signal and voltage input signal were collected and regulated by Clampfit9.2 software (Axon Corporation, San Jose, CA, USA), which was pre-recorded according to the protocol of I_{Na} recording.

While recording the I_{Na}, the potential was maintained at –80 mV under the voltage clamp mode, and a depolarization pulse of 50 ms was applied to record I_{Na} at each voltage.

In order to plot the I_{Na} current-voltage curve (I-Vcurve), the potential was kept at –80 mV and applied continuously for 50 ms under the voltage clamp mode. With the depolarization pulse set from –70 mV to +40 mV, and the step at 10 mV, the I_{Na} at each voltage was recorded.

To evaluate the steady-state activity (SSA) of I_{Na}, the potential was maintained at –80 mV for 500 ms. With the depolarization pulse set at –70 mV to +40 mV, and the step at 10 mV, the I_{Na} was recorded. After the current was standardized, the curve of standardized current versus stimulation pulses under each voltage was plotted. The semi-activated voltage ($V_{1/2,act}$) and the slope of activation curve (K_{act}) were obtained by curve fitting with the Boltzmann equation.

To evaluate the steady-state inactivity (SSI) of I_{Na}, a set of parameters such as a rapid pulse of –120 mV to –20 mV, a step of 10 mV, and 1000 ms were applied at a potential of –90 mV. Then, for each pulse followed by a test pulse of a fixed depolarization to –35 mV for 50 ms, the I_{Na} was recorded. The half-inactivation voltage ($V_{1/2}$, I_{Nact}) and the slope of inactivation curve (K_{INact}) were obtained by curve fitting with the Boltzmann equation.

In order to plot the recovery curve of I_{Na}, double stimulation mode was adopted, while applying an array of parameters: voltage clamp at –120 mV, conditional pulse and test pulse both at –35 mV, and 50 ms, and gradually increasing the interval between the two pulses (20, 40, 80, 160, 320, 640 ms). The curve was plotted with the ratio of I_{Na} between the test pulse and the conditional pulse and the time interval.

Statistical Analysis

Patch clamp graphics were collected and extracted by pCLAMP 9.2 software (Axon Corporation, San Jose, CA, USA), and corresponding voltage (V), current (I), membrane capacitance (Cm), current density (I/Cm), and relative current (I/I_{max}) of each data were recorded. The steady-state activation curve and steady-state deactivation curve were fitted to the Boltzmann equation, and the post-deactivation recovery curve was fitted to the exponential equation. The calculated data were processed by Origin 8.5 software (OriginLab Corporation, Northampton, MA, USA), and the current curve was drawn. Image Pro Plus software (National Institutes of Health, Bethesda, MD, USA) was used to analyze the gray values of strips obtained in the Western blotting experiment, and the gray values were standardized according to internal parameters. *t*-test was used for data comparison between groups, one-way analysis of variance (ANOVA) was used for data comparison between multiple groups, with Student-Newman-Keuls (SNK)-q test serving as the post-hoc test for pairwise comparison. SPSS 15.0 (IBM Corporation, Armonk, NY, USA) was used for statistical analysis. All data in this paper are expressed as mean ± standard deviation. $p < 0.05$ was considered statistically significant.

Results

Effects of Hypoxia on I_{Na} of HL-1 Cells

Compared with the NO group, the HO group experienced a significant increase in I_{Na} peak current amplitude after the hypoxia strategy was adopted (Fig. 1A). The I_{Na} peak current density was also significantly higher than that in NO (Fig. 1B, n = 15, $p < 0.01$).

A series of I_{Na} currents were induced by a series of stimulus pulses, and the increase of current in the HO group

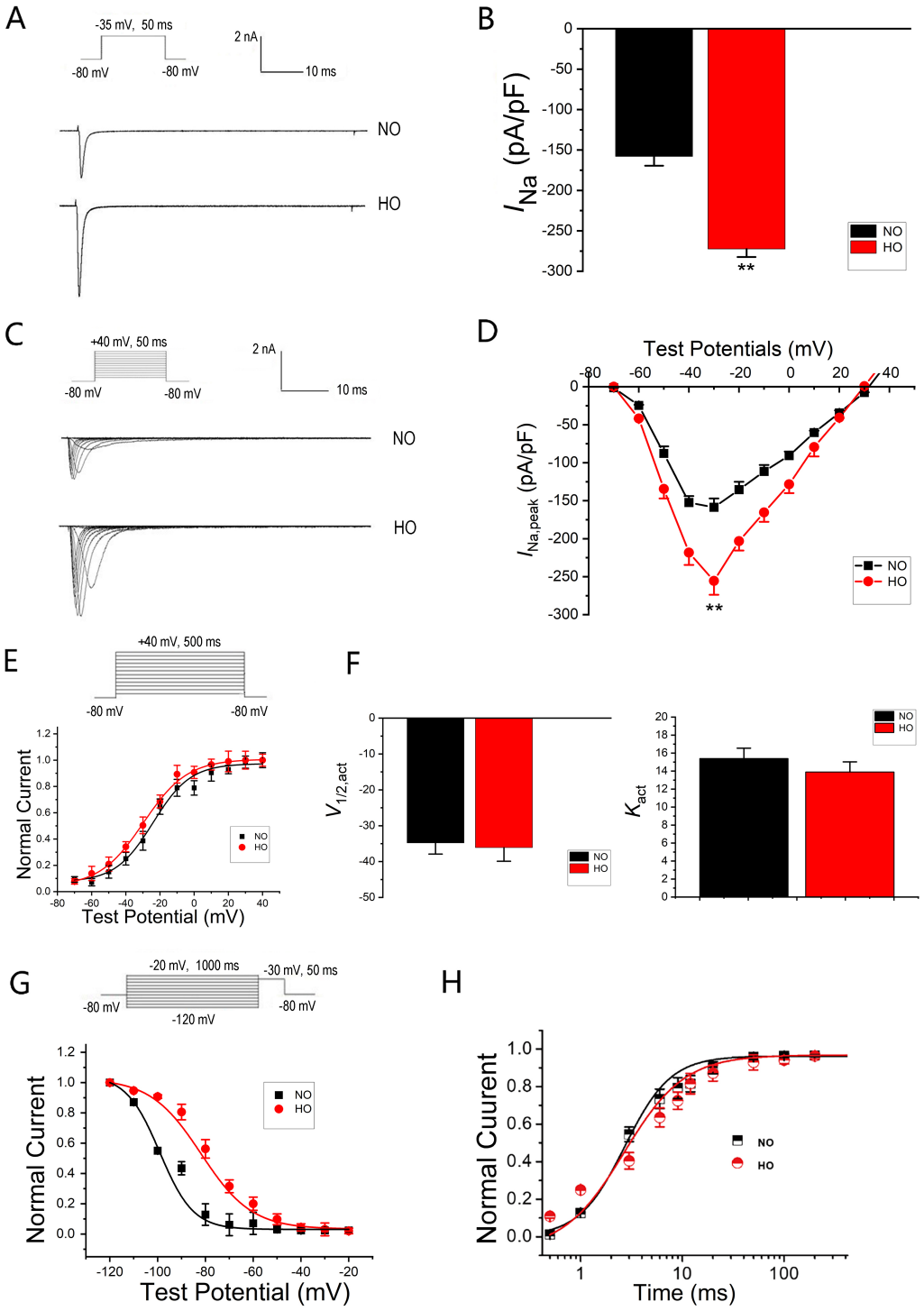

Fig. 1. Effect of hypoxia treatment on sodium ion channel current (I_{Na}) and voltage-gated Na^+ channels (Nav1.5) channel gating mechanism characteristics. (A) The amplitude of the I_{Na} peak current in HL-1 cells was significantly increased under hypoxic conditions. (B) Influence of hypoxia on I_{Na} peak current density. (C) Original recording diagram of the effect of hypoxia on I_{Na}. (D) Effect of hypoxia on the I_{Na} voltage-current curve (I-V). The I-V curve depicts a significant increase in current in the hypoxia group (HO) group compared to the normoxia group (NO) group, with a significant increase in I_{Na} in the stimulation range of –50 mV to 0 mV, especially near the peak. (E) Hypoxic conditions affect the steady-state activation curve of HL-1 cell I_{Na}. (F) Changes in steady-state activation parameters under hypoxic conditions (the semi-activation voltage ($V_{1/2,act}$) and the activation curve slope (K_{act})). (G) The steady-state inactivation curve of I_{Na} from HL-1 cells under hypoxic conditions. (H) Recovery curve of HL-1 cell I_{Na} under hypoxic conditions after inactivation. Data are expressed as the means ± S.D. Notes: n = 15, $^{**}p < 0.01$; student's *t*-test.

(–272.5 ± 9.8 pA/pF) was more obvious than that in the NO group (–158.2 ± 11.5 pA/pF, n = 15, $p < 0.01$, Fig. 1C). The voltage-current curve (I-V) of I_{Na} was plotted by the current density recorded at each test potential and the corresponding potential. It was found that in the range of –50 mV to 0 mV, the I_{Na} increased significantly under hypoxic condition, and this effect was particularly significant near the peak (Fig. 1D).

Gating Mechanism Affecting the Increase of I_{Na} under Hypoxia

The influence of hypoxia on I_{Na} homeostasis activation was explored following an extended stimulation of HL-1 cells to fully activate their sodium ion channels. The current and maximum current recorded at each stimulus potential were standardized, and the I_{Na} current steady-state activation curve was plotted with the standardized current versus the stimulus pulses at each voltage (Fig. 1E). The results showed that the steady-state activation curve shifted slightly to the left in the HO group compared with the NO group. At the same time, hypoxia might slightly accelerate the steady-state activation process, but the movement amplitude was relatively small, with limited effect.

The above-mentioned curves were fitted by Boltzmann equation ($G/G_{max} = 1/\{1 + \exp[(v0.5 – VM)/k]\}$), and the semi-activation voltage ($V_{1/2,act}$) and activation curve slope (K_{act}) were calculated. The results, as presented in Fig. 1F, showed that the values of $V_{1/2,act}$ (NO group: $V_{1/2,act}$: –34.8 ± 3.1 mV, HO group: $V_{1/2,act}$: –36.1 ± 3.8 mV, n = 15, $p > 0.05$) and K_{act} had undergone little change, suggesting that hypoxia treatment had limited influence on the steady-state activation process of sodium ion channel, and the effect of hypoxia on increasing peak I_{Na} was minimally associated with steady-state activation.

The steady-state inactivation of the sodium ion channel was investigated by using the dual stimulus mode (conditional stimulus + test stimulus). The residual current recorded at each stimulus potential and the maximum residual current were standardized. The steady-state inactivation curve of I_{Na} was obtained by plotting the standardized residual current versus the stimulus voltage under each condition. The results showed that the steady-state inactivation curve shifted significantly to the right for the HO group ($V_{1/2,inact}$: –72.3 ± 7.1 mV), as compared with the NO group ($V_{1/2,inact}$: –94.3 ± 6.7 mV, n = 15, $p < 0.01$, Fig. 1G).

Dual stimulation mode was employed to study the effect of hypoxia on the recovery time constant of sodium ion channel inactivation. The time constant of kinetic recovery after inactivation was calculated by a single exponential ($I/I_{max} = I0 + AEXP(t/\tau)$). It was found that hypoxia treatment caused a slight left shift in the recovery curve after inactivation, but there was no statistical significance (Fig. 1H).

Expression and Distribution of Nav1.5 Channel and ANK-G in HL-1 Cells under Hypoxia

Immunofluorescence and Western blotting were used to detect the distribution and expression of Nav1.5 channel proteins in the cell membrane to study the mechanism of regulating Nav1.5 channel in cardiomyocytes under hypoxia.

The Western blotting results showed that the protein levels of ANK-G and Nav1.5 channel in HL-1 cells of the HO group increased significantly compared to the NO group (Fig. 2A, n = 3, $p < 0.001$), suggesting that ANK-G and Nav1.5 channel proteins could be increased in anoxic environment. This is probably the cause of electrophysiological changes in HL-1 cells under hypoxic environment.

Immunofluorescence results (Fig. 2B, **Supplementary Materials 3,4**) showed that the expression of ANK-G in the membrane and the cell increased under hypoxia, and the Nav1.5 channel expression showed a significant increase, featuring channel redistribution, in the membrane, confirming the elevated level of channel protein migration and the increased maturation and synthesis of this protein under hypoxia.

Effects of ANK-G on Expression and Distribution of Nav1.5 Channel Protein under Hypoxia

In this experiment, the expression of *ANK-G* and the expression and distribution of Nav1.5 channel in the cell membrane, in the context of hypoxia, were also detected. By manipulating the expression of *ANK-G*, we found that hypoxia required the participation of *ANK-G* in changing the expression of Nav1.5.

Western blotting results showed that ANK-G protein levels of HL-1 cells in the ANK-G group were significantly increased (n = 3, $p < 0.01$). But the ANK-G protein levels of the sh*ANK-G* group decreased significantly (n = 3, $p < 0.001$). This indicates that the lentivirus transfection performed in this study was successful (Fig. 2C).

The Nav1.5 channel protein levels of the ANK-G group were significantly elevated (n = 3, $p < 0.001$). But the Nav1.5 channel protein levels of the sh*ANK-G* group were significantly suppressed (n = 3, $p < 0.0001$). This suggests that increased *ANK-G* expression could increase Nav1.5 channel protein level under hypoxic conditions (Fig. 2C).

Confocal microscopy scanning (Fig. 2D, **Supplementary Materials 3,4**) showed that the fluorescence levels in the ANK-G group increased significantly, with the fluorescence accumulating at the cell membrane. In the sh*ANK-G* group, fluorescence levels decreased significantly. The successful *ANK-G* overexpression or knockdown indicated that the lentiviral infection was effective.

Confocal microscopy showed that the fluorescence levels in the ANK-G groups increased significantly, with the fluorescence being prominently intense at the cell membrane (Fig. 2D, **Supplementary Materials 3,4**). In the

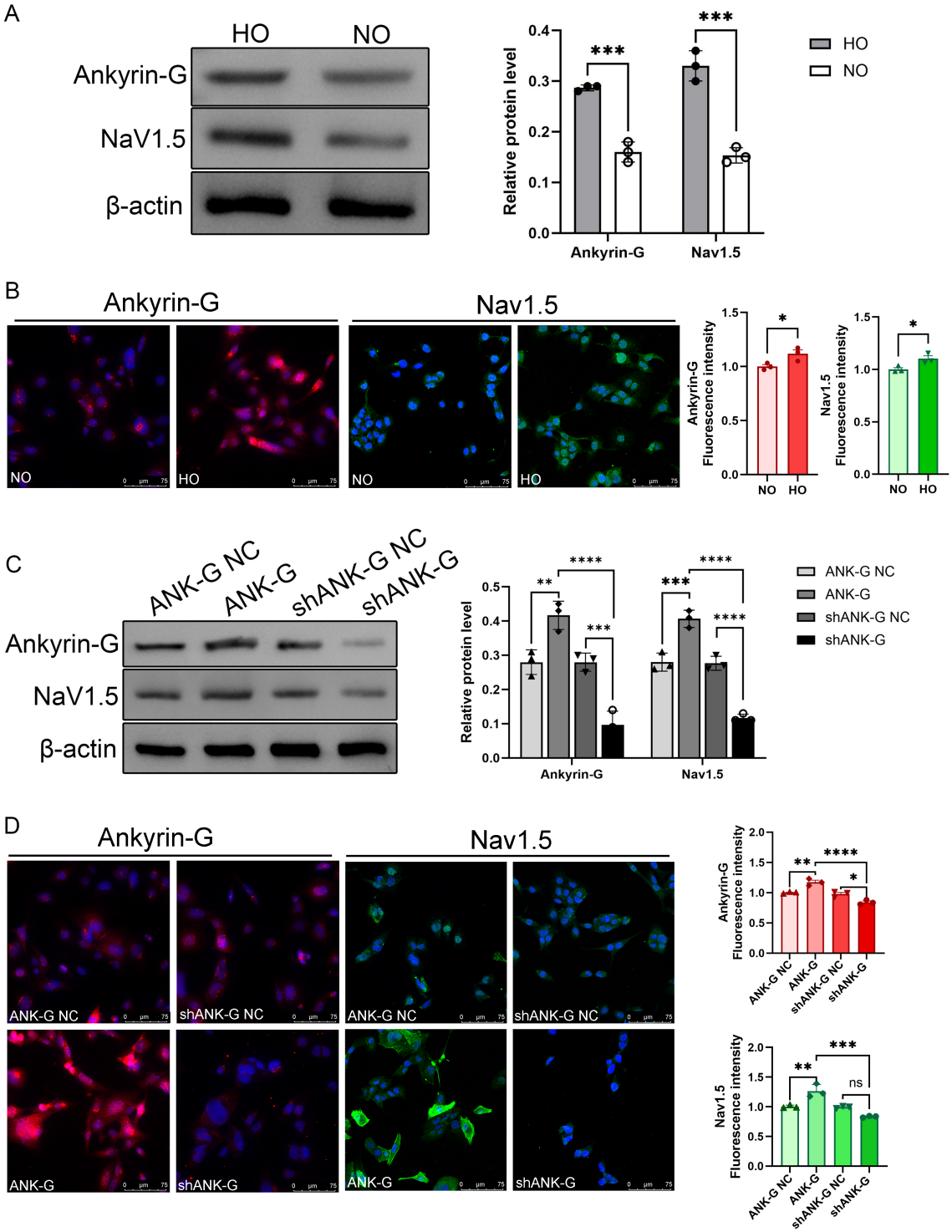

Fig. 2. The expression and distribution of Nav1.5 channel and ankyrin-G (ANK-G) in HL-1 cells (A,B) and the effect of ANK-G on expression and distribution of Nav1.5 channel protein (C,D) under hypoxic conditions. (A) Hypoxia affects the expression levels of *ANK-G* and Nav1.5 channel protein in HL-1 cells. (B) Hypoxia affects the expression of ANK-G and Nav1.5 channel protein in HL-1 cells (scale bar: 75 µm; magnification: ×40). (C) The expression levels of ANK-G and Nav1.5 channel protein in each group. (D) Immunofluorescence staining of ANK-G and Nav1.5 channel protein for each group (scale bar: 75 µm; magnification: ×40). Data are expressed as mean ± S.D. Notes: n = 3; ns, non-significant, *$p < 0.05$, **$p < 0.01$, ***$p < 0.001$, ****$p < 0.0001$; student's *t*-test (A), and one-way analysis of variance (ANOVA) (C). ANK-G NC, *ANK-G*-overexpressing hypoxia-negative group.

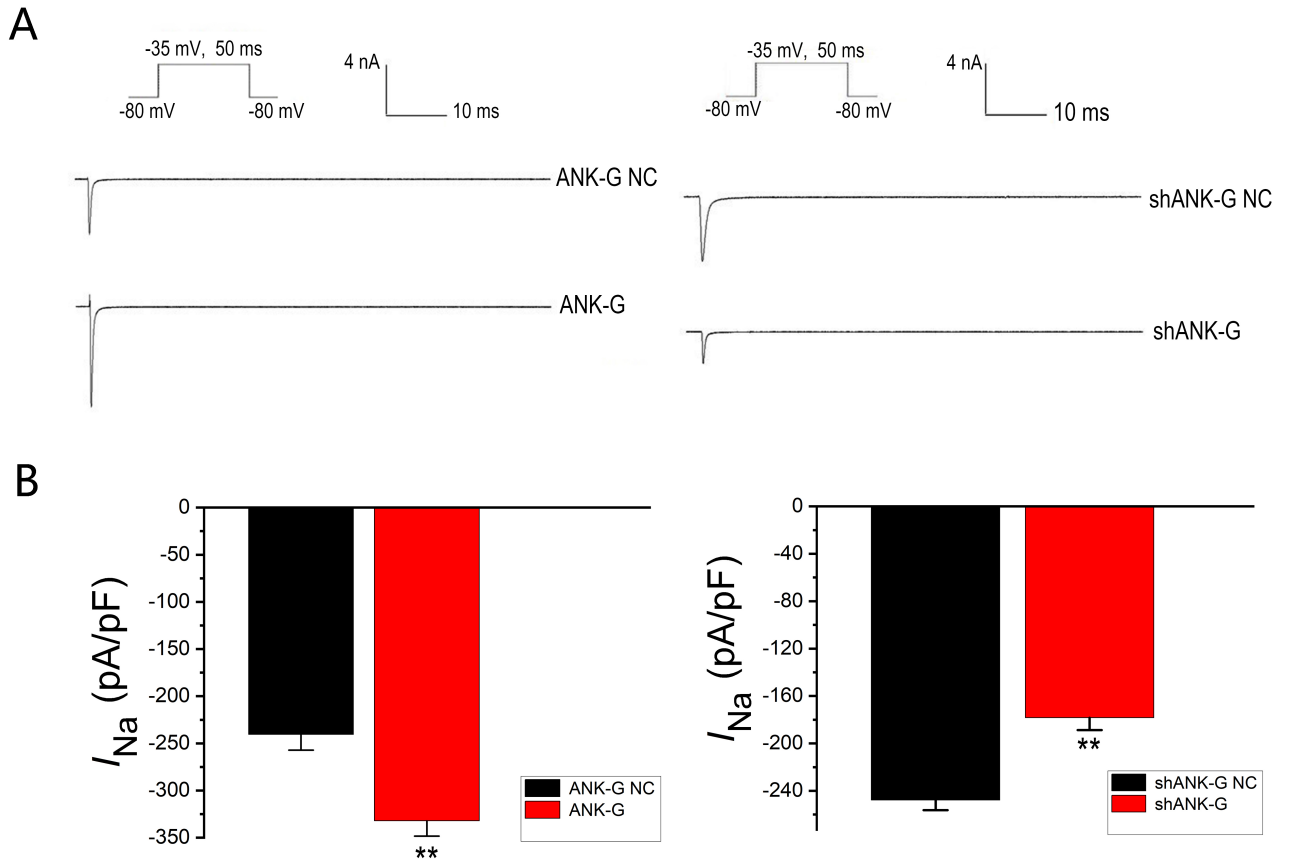

Fig. 3. Effect of *ANK-G* on I_{Na} under hypoxic conditions. (A) *ANK-G* affects the amplitude of I_{Na} in HL-1 cells under hypoxic conditions. (B) *ANK-G* affects the I_{Na} peak current density of HL-1 cells under hypoxic conditions. Data are expressed as mean ± S.D. Notes: n = 15, $^{**}p < 0.01$; student's *t*-test.

sh*ANK-G* group, Nav1.5 channel fluorescence was obviously weakened. This suggests that *ANK-G* could increase the distribution of Nav1.5 channel in the cell membrane under hypoxia.

Effects of ANK-G on I_{Na} under Hypoxia

The overexpression of *ANK-G* increased the amplitude of I_{Na} peak current of HL-1 cells under hypoxia, whereas the silencing of *ANK-G* decreased the amplitude of I_{Na} peak current significantly (Fig. 3A, n = 15, $p < 0.01$).

The overexpression of *ANK-G* increased the peak current density of I_{Na} (from –240.6 ± 16.5 pA/pF to –332.1 ± 16.3 pA/pF) at –35 mV depolarization voltage (n = 15, $p <$ 0.01). Under the same conditions, silencing *ANK-G* gene significantly reduced the peak current density of I_{Na} (from –247.8 ± 8.5 pA/pF to –178.3 ± 10.4 pA/pF) at –35 mV depolarization voltage (Fig. 3B, n = 15, $p < 0.01$).

Discussion

Abnormal expression or function of various ion channels in cardiomyocytes serves as the prime pathophysiological trigger of various types of arrhythmias. Hypoxia can cause aberrations to sodium ion channels in the myocardium, resulting in cardiac electrophysiological abnormalities. Relevant studies suggested that hypoxia could continuously enhance I_{Na} of cardiomyocytes and lead to arrhythmias by prolonging the duration of action potential, but the specific gating mechanism was not thoroughly studied.

In this study, it was found that the I_{Na} current amplitude and density of HL-1 atrial myocytes were increased after experiencing acute hypoxia for 2 h. This indicates that acute hypoxia could affect the sodium current of HL-1 cells, making them more sensitive and volatile.

The late sodium current was a component of the I_{Na}, which lasted for a long time after the rapid inactivation of components [16]. In all species and all types of cardiomyocytes, the amplitude of late sodium current was relatively small compared to that of the fast sodium current, but it contributed greatly to the shape and duration of action potential [17]. Acute cardiac hypoxia increased the late sodium current in the myocardium, possibly due to hypoxia-induced rapid ubiquitin activation of Nav1.5 channels, associated with their reopening during inactivity [18].

However, a study on rats found that AMP-activated protein kinase (AMPK) mediated autophagy of Nav1.5 channel during cardiac ischemia/reperfusion injury, led to

a significant decrease in Nav1.5 channel protein level [19]. Chronic intermittent hypoxia also reduced Nav1.5 channel expression and I_{Na} amplitude and current density in rat myocardium [20]. These findings, however, were contrary to the results of this study focusing on acute hypoxia. Thus, we speculate that different hypoxia modes would elicit distinctly different effects on myocardial I_{Na}.

In cardiomyocytes, action potentials are triggered by sodium ion influx through voltage-gated Na^+ channels [21]. Voltage-gated Na^+ channels (Nav1.5) play a leading role in the upward movement of excitable cell action potentials, while non-inactivated I_{Na} affects the shape and duration of action potentials [22].

The altered I_{Na} is not only a function of the deactivation mechanics of the extended individual Na channels, but also correlates with the number and distribution of Nav1.5 channels. This experiment confirmed that hypoxia slowed down the inactivation kinetics of the I_{Na}, without affecting steady-state activation and post-inactivation recovery much, suggesting that the mechanism by which hypoxia alters I_{Na} is closely related to the deactivation of Nav1.5 channel.

Electrophysiological evidence derived from research on HEK 293 cells suggested that hypoxia changes the gating mechanism of Nav1.5 channel, possibly related to the expression of channels driven by exogenous promoters and to post-transcriptional modification of Nav1.5 channel [23]. There was evidence that the transcription factor Tbx5 was associated with *SCN5A* and could control the genesis of the mouse's heart and drive the expression of *SCN5A* [24].

SCN5A is a key gene involved in encoding Nav1.5 channel [25]. It has been found that Nup107 overexpression induced the expression of *SCN5A*-encoded protein and significantly increased the I_{Na}, suggesting that nucleoporin 107 of cardiomyocytes interacted with *SCN5A* mRNA when it passed through the nuclear pore under hypoxia, and then regulated Nav1.5 channels in cardiomyocytes [26]. However, a recent study on the mechanism of arrhythmia after myocardial infarction found the increased expression of already-recognized hypoxia response factors during cardiac ischemia, such as hypoxia-inducible factor-1 α and nuclear factor kappa-B (NF-κB) [27,28], which upregulated the MIR448 level, thereby inhibiting the expression of *SCN5A* and I_{Na} elevation [29]. This finding was contradictory to the results of this study, possibly because the whole organ after myocardial infarction was studied in the published research, which focused on the adjustment during the stage of collective compensation. However, the current study was conducted on individual cells exposed to acute hypoxia, reflected the stress reaction of atrial muscle cells under hypoxic environment. The specific regulatory mechanism still warrants further research.

ANK-G is a protein connecting membrane proteins to the underlying cytoskeletal network. ANK-G regulates cardiac excitability by coordinating the intercalated disc signaling platform [13]. There is conclusive evidence that direct interaction between Nav1.5 channel and ANK-G is required for Nav1.5 channel expression on the surface of cardiomyocytes [30]. Related study further revealed that the expression of Nav1.5 channel was reduced in cardiomyocytes with reduced ANK-G, the membrane targeting of Nav1.5 channel was abnormal, and the current density of Na^+ channel was reduced [31].

In this study, lentivirus was used to generate both *ANK-G*-overexpressing and -silenced HL-1 cell-based models. It was found that *ANK-G* gene had a direct regulatory effect on I_{Na}, by changing the amplitude and peak current density of I_{Na}. Overexpression of *ANK-G* could amplify the effect of hypoxia on I_{Na} in HL-1 cells, while silencing *ANK-G* could reverse such effect. The mechanism of hypoxia affecting I_{Na} at cellular and molecular levels, along with the regulatory effect of *ANK-G* on the expression and distribution of Nav1.5 channel, was explored in thus study.

This study is not without limitations. The current study did not investigate the mechanism of hypoxia regulation at the genetic level, nor did it further decipher the effect of hypoxia on the heart of animal models, at multiple levels, to explore the electrophysiological mechanism of hypoxia and ANK-G regulation of atrial myocytes. In this study, the I_{Na} was the only ion channel current detected. In order to understand the electrophysiological properties of atrial myocytes under the condition of hypoxia, current changes in the calcium ion channel and potassium ion channel should be investigated in future studies.

Early effective improvement of the hypoxic environment in myocytes (through thrombolytic, interventional recanalization) and reversal of abnormal electrophysiology of myocardium could improve or even halt the occurrence of arrhythmias such as AF. In addition, the discovery of the regulatory effect of *ANK-G* on Nav1.5 channel in this study paves the way for reversing I_{Na} via ANK-G in the context of hypoxia as a potential therapeutic target for atrial fibrillation (AF).

Conclusions

Under hypoxic conditions, the gating mechanism of I_{Na} is related to steady-state inactivation, but not associated with steady-state activation and recovery after inactivation. Furthermore, hypoxia leads to the elevated level of ANK-G protein in HL-1 cells, which promotes the redistribution of Nav1.5 channel protein in the cell membrane, thereby increasing I_{Na} peak current amplitude and density.

Availability of Data and Materials

All datasets analyzed to support the findings of the current study are available from the corresponding authors upon reasonable request.

Author Contributions

Conception and design of research: XC, YL; SM, WL performed experiments; SY, PX, CW analyzed data; XC, YL, SY, YW, HH interpreted results of experiments; PX, SY prepared figures; SM, PX, YW drafted manuscript. All authors contributed significantly to editorial changes of important content. All authors read and approved the final version of the manuscript. All authors have participated sufficiently in the work and agreed to be accountable for all aspects of the work.

Ethics Approval and Consent to Participate

Experimental protocol was approved by the 82nd Group Army Hospital of the Chinese PLA (Approval Number: 202011).

Acknowledgment

Not applicable.

Funding

This study was supported by grants from the Hebei Province Medical Science Research Project (20210744), the Special Fund for Team of Sports Induced Heart Injury Prevention and Treatment in Military, the Key Specialty Training Program of Clinical Military Medicine, the Theater Army Medical Autonomous Research Project (2023LC10), Army Logistics Autonomous Research Program (ZLJ22J027) and the Baoding Science and Technology Plan Project (2241ZF389).

Conflict of Interest

The authors declare no conflict of interest.

Supplementary Material

Supplementary material associated with this article can be found, in the online version, at https://doi.org/10.24976/Discov.Med.202436190.201.

References

[1] Pandit SV, Workman AJ. Atrial Electrophysiological Remodeling and Fibrillation in Heart Failure. Clinical Medicine Insights. Cardiology. 2016; 10: 41–46.

[2] Syeda F, Holmes AP, Yu TY, Tull S, Kuhlmann SM, Pavlovic D, *et al*. PITX2 Modulates Atrial Membrane Potential and the Antiarrhythmic Effects of Sodium-Channel Blockers. Journal of the American College of Cardiology. 2016; 68: 1881–1894.

[3] Takla M, Huang CLH, Jeevaratnam K. The cardiac CaMKII-$Na_v1.5$ relationship: From physiology to pathology. Journal of Molecular and Cellular Cardiology. 2020; 139: 190–200.

[4] Xiong H, Yang Q, Zhang X, Wang P, Chen F, Liu Y, *et al*. Significant association of rare variant p.Gly8Ser in cardiac sodium channel β4-subunit SCN4B with atrial fibrillation. Annals of Human Genetics. 2019; 83: 239–248.

[5] Cho KW, Lee J, Kim Y. Genetic Variations Leading to Familial Dilated Cardiomyopathy. Molecules and Cells. 2016; 39: 722–727.

[6] Strege PR, Mercado-Perez A, Mazzone A, Saito YA, Bernard CE, Farrugia G, *et al*. *SCN5A* mutation G615E results in $Na_V1.5$ voltage-gated sodium channels with normal voltage-dependent function yet loss of mechanosensitivity. Channels (Austin, Tex.). 2019; 13: 287–298.

[7] Han D, Tan H, Sun C, Li G. Dysfunctional Nav1.5 channels due to SCN5A mutations. Experimental Biology and Medicine (Maywood, N.J.). 2018; 243: 852–863.

[8] Veerman CC, Wilde AAM, Lodder EM. The cardiac sodium channel gene SCN5A and its gene product NaV1.5: Role in physiology and pathophysiology. Gene. 2015; 573: 177–187.

[9] Jenkins PM, Vasavda C, Hostettler J, Davis JQ, Abdi K, Bennett V. E-cadherin polarity is determined by a multifunction motif mediating lateral membrane retention through ankyrin-G and apical-lateral transcytosis through clathrin. The Journal of Biological Chemistry. 2013; 288: 14018–14031.

[10] Xiao YF, Ma L, Wang SY, Josephson ME, Wang GK, Morgan JP, *et al*. Potent block of inactivation-deficient Na+ channels by n-3 polyunsaturated fatty acids. American Journal of Physiology. Cell Physiology. 2006; 290: C362–C370.

[11] Jiang D, Shi H, Tonggu L, Gamal El-Din TM, Lenaeus MJ, Zhao Y, *et al*. Structure of the Cardiac Sodium Channel. Cell. 2020; 180: 122–134.e10.

[12] Shy D, Gillet L, Abriel H. Cardiac sodium channel NaV1.5 distribution in myocytes via interacting proteins: the multiple pool model. Biochimica et Biophysica Acta. 2013; 1833: 886–894.

[13] Makara MA, Curran J, Lubbers ER, Murphy NP, Little SC, Musa H, *et al*. Novel Mechanistic Roles for Ankyrin-G in Cardiac Remodeling and Heart Failure. JACC. Basic to Translational Science. 2018; 3: 675–689.

[14] Makara MA, Curran J, Little SC, Musa H, Polina I, Smith SA, *et al*. Ankyrin-G coordinates intercalated disc signaling platform to regulate cardiac excitability in vivo. Circulation Research. 2014; 115: 929–938.

[15] Dun W, Lowe JS, Wright P, Hund TJ, Mohler PJ, Boyden PA. Ankyrin-G participates in INa remodeling in myocytes from the border zones of infarcted canine heart. PloS One. 2013; 8: e78087.

[16] Li F, Li ML, Wu L. Late Sodium Current-Associated Cardiac Arrhythmias in Acquired Cardiovascular Diseases. Progress in Physiological Science. 2020; 51: 321–326. (In Chinese)

[17] Antzelevitch C, Nesterenko V, Shryock JC, Rajamani S, Song Y, Belardinelli L. The role of late I Na in development of cardiac arrhythmias. Handbook of Experimental Pharmacology. 2014; 221: 137–168.

[18] Plant LD, Xiong D, Romero J, Dai H, Goldstein SAN. Hypoxia Produces Pro-arrhythmic Late Sodium Current in Cardiac Myocytes by SUMOylation of $Na_V1.5$ Channels. Cell Reports. 2020; 30: 2225–2236.e4.

[19] Liu X, Chen Z, Han Z, Liu Y, Wu X, Peng Y, *et al*. AMPK-mediated degradation of Nav1.5 through autophagy. FASEB Journal: Official Publication of the Federation of American Societies for Experimental Biology. 2019; 33: 5366–5376.

[20] Zhang K, Ma Z, Song C, Duan X, Yang Y, Li G. Role of ion channels in chronic intermittent hypoxia-induced atrial remodeling in rats. Life Sciences. 2020; 254: 117797.

[21] Nowak MB, Greer-Short A, Wan X, Wu X, Deschênes I, Weinberg SH, *et al*. Intercellular Sodium Regulates Repolarization in Cardiac Tissue with Sodium Channel Gain of Function. Biophysical Journal. 2020; 118: 2829–2843.

[22] Chen ZP, Guang XF. Advances in the pathogenesis of ion chan-

nels in arrhythmias. Forum on Primary Medicine. 2015; 19: 2667–2668. (In Chinese)

[23] Fearon IM, Brown ST. Acute and chronic hypoxic regulation of recombinant hNa(v)1.5 alpha subunits. Biochemical and Biophysical Research Communications. 2004; 324: 1289–1295.

[24] Nieto-Marín P, Tinaquero D, Utrilla R, Cebrián J, González-Guerra A, Crespo-García T, *et al*. Tbx5 variants disrupt Nav1.5 function differently in patients diagnosed with Brugada or Long QT Syndrome. Cardiovascular Research. 2022; 118: 1046–1060.

[25] Li W, Yin L, Shen C, Hu K, Ge J, Sun A. *SCN5A* Variants: Association with Cardiac Disorders. Frontiers in Physiology. 2018; 9: 1372.

[26] Guan Y, Gao X, Tang Q, Huang L, Gao S, Yu S, *et al*. Nucleoporin 107 facilitates the nuclear export of Scn5a mRNA to regulate cardiac bioelectricity. Journal of Cellular and Molecular Medicine. 2019; 23: 1448–1457.

[27] Belaiba RS, Bonello S, Zähringer C, Schmidt S, Hess J, Kietzmann T, *et al*. Hypoxia up-regulates hypoxia-inducible factor-1alpha transcription by involving phosphatidylinositol 3-kinase and nuclear factor kappaB in pulmonary artery smooth muscle cells. Molecular Biology of the Cell. 2007; 18: 4691–4697.

[28] Fitzpatrick SF, Tambuwala MM, Bruning U, Schaible B, Scholz CC, Byrne A, *et al*. An intact canonical NF-κB pathway is required for inflammatory gene expression in response to hypoxia. Journal of Immunology (Baltimore, Md.: 1950). 2011; 186: 1091–1096.

[29] Kang GJ, Xie A, Liu H, Dudley SC, Jr. MIR448 antagomir reduces arrhythmic risk after myocardial infarction by upregulating the cardiac sodium channel. JCI Insight. 2020; 5: e140759.

[30] Bennett V, Healy J. Being there: cellular targeting of voltage-gated sodium channels in the heart. The Journal of Cell Biology. 2008; 180: 13–15.

[31] Lowe JS, Palygin O, Bhasin N, Hund TJ, Boyden PA, Shibata E, *et al*. Voltage-gated Nav channel targeting in the heart requires an ankyrin-G dependent cellular pathway. The Journal of Cell Biology. 2008; 180: 173–186.